Title

A stromal progenitor and ILC2 niche promotes muscle eosinophilia and fibrosis-associated gene expression

Journal

Cell Reports, 35(2)

ISSN

2639-1856

Authors

Kastenschmidt, Jenna M

Coulis, Gerald

Farahat, Philip K

et al.

Publication Date

2021-04-01

DOI

10.1016/j.celrep.2021.108997

Peer reviewed

HHS Public Access

Author manuscript

Cell Rep. Author manuscript; available in PMC 2021 May 17.

Published in final edited form as:

Cell Rep. 2021 April 13; 35(2): 108997. doi:10.1016/j.celrep.2021.108997.

A stromal progenitor and ILC2 niche promotes muscle eosinophilia and fibrosis-associated gene expression

Jenna M. Kastenschmidt[1,2], **Gerald Coulis**[1,2], **Philip K. Farahat**[1,2], **Phillip Pham**[1], **Rodolfo Rios**[1], **Therese T. Cristal**[1], **Ali H. Mannaa**[1], **Rachel E. Ayer**[1], **Rayan Yahia**[1], **Archis A. Deshpande**[1], **Brandon S. Hughes**[1], **Adam K. Savage**[3,4], **Carlee R. Giesige**[5,6], **Scott Q. Harper**[5,6,7], **Richard M. Locksley**[3], **Tahseen Mozaffar**[2,8,9,10], **S. Armando Villalta**[1,2,8,11,*]

[1]Department of Physiology and Biophysics, University of California Irvine, Irvine, CA, USA

[2]Institute for Immunology, University of California Irvine, Irvine, CA, USA

[3]Howard Hughes Medical Institute, University of California San Francisco, San Francisco, CA, USA

[4]Departments of Medicine and Microbiology & Immunology, University of California San Francisco, San Francisco, CA, USA

[5]Biomedical Sciences Graduate Program, The Ohio State University, Columbus, OH, USA

[6]Center for Gene Therapy, The Research Institute at Nationwide Children's Hospital, Columbus, OH, USA

[7]Department of Pediatrics, The Ohio State University, Columbus, OH, USA

[8]Department of Neurology, University of California Irvine, Irvine, CA, USA

[9]Department of Orthopaedic Surgery, University of California Irvine, Irvine, CA, USA

[10]Department of Pathology and Laboratory Medicine, University of California Irvine, Irvine, CA, USA

[11]Lead contact

SUMMARY

Despite the well-accepted view that chronic inflammation contributes to the pathogenesis of Duchenne muscular dystrophy (DMD), the function and regulation of eosinophils remain an unclear facet of type II innate immunity in dystrophic muscle. We report the observation that

*Correspondence: armando.villalta@uci.edu.

AUTHOR CONTRIBUTIONS

The study was designed by S.A.V. and J.M.K. J.M.K. performed and analyzed experiments with contributions from S.A.V., G.C., P.K.F., P.P., R.R., T.T.C., A.H.M., R.E.A., R.Y., A.A.D., B.S.H., A.K.S., and C.R.G. T.M., R.M.L., and S.Q.H. provided mouse models, consultation, and human specimens. J.M.K. and S.A.V. prepared the manuscript, and all authors approved the final manuscript version.

DECLARATION OF INTERESTS

The authors declare no competing interests.

SUPPLEMENTAL INFORMATION

Supplemental information can be found online at https://doi.org/10.1016/j.celrep.2021.108997.

group 2 innate lymphoid cells (ILC2s) are present in skeletal muscle and are the principal regulators of muscle eosinophils during muscular dystrophy. Eosinophils were elevated in DMD patients and dystrophic mice along with interleukin (IL)-5, a major eosinophil survival factor that was predominantly expressed by muscle ILC2s. We also find that IL-33 was upregulated in dystrophic muscle and was predominantly produced by fibrogenic/adipogenic progenitors (FAPs). Exogenous IL-33 and IL-2 complex (IL-2c) expanded muscle ILC2s and eosinophils, decreased the cross-sectional area (CSA) of regenerating myofibers, and increased the expression of genes associated with muscle fibrosis. The deletion of ILC2s in dystrophic mice mitigated muscle eosinophilia and impaired the induction of IL-5 and fibrosis-associated genes. Our findings highlight a FAP/ILC2/eosinophil axis that promotes type II innate immunity, which influences the balance between regenerative and fibrotic responses during muscular dystrophy.

In brief

Immune cells that comprise type II innate immunity coalesce to regulate tissue repair and fibrosis. Kastenschmidt et al. report that ILC2s reside in skeletal muscle, are activated in muscular dystrophy, and promote muscle eosinophilia. Stromal progenitors expressed IL-33, which expanded ILC2s and promoted a transcriptional program associated with muscle fibrosis.

Graphical Abstract

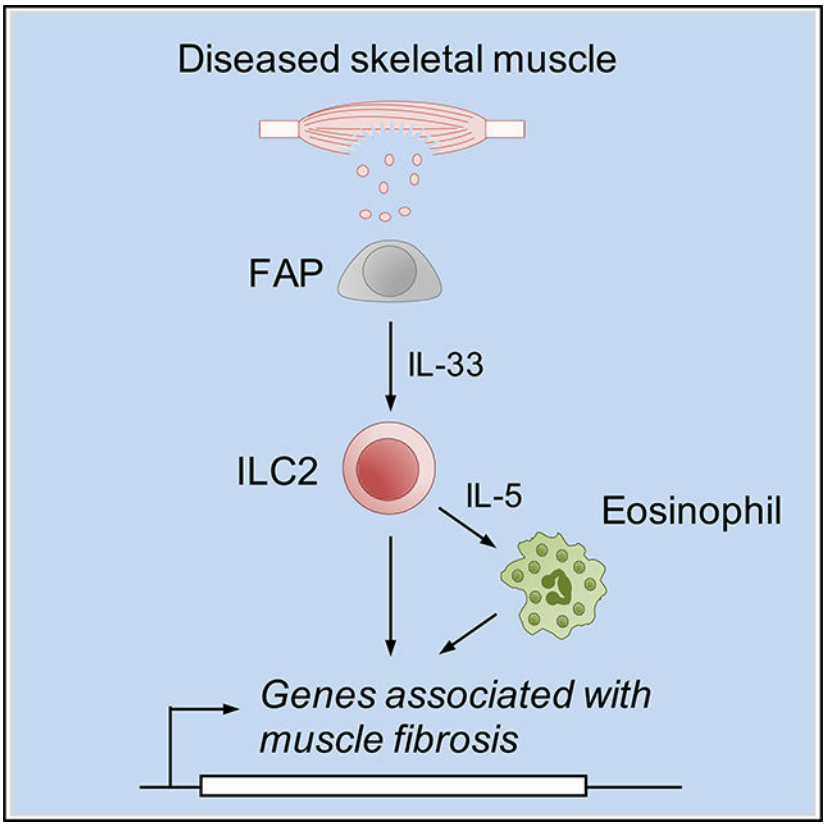

INTRODUCTION

Chronic inflammation is a major pathological process contributing to the progression and severity of Duchenne muscular dystrophy (DMD), a fatal monogenic muscle disorder attributed to dystrophin mutations (Hoffman et al., 1987). Several studies directed at establishing a causal link between muscular dystrophy and muscle inflammation have revealed a complex dysregulation of the immune response to muscle damage (Villalta et al., 2015). A critical facet of this response is the activation of type II innate immunity, which includes the production of cytokines, including interleukin (IL)-4, IL-5, and IL-13, and increased M2-like macrophages and eosinophils (Gieseck et al., 2018). Studies of type II immunity in acute muscle injury indicate that eosinophils promote muscle regeneration (Heredia et al., 2013). The role of eosinophils in muscular dystrophy, however, is much more complex. The depletion of eosinophils with a CCR3-specific antibody caused a reduction in myofiber injury in the mdx mouse model of DMD (Wehling-Henricks et al., 2008). In contrast, genetic ablation of eosinophils in mdx mice did not influence muscle damage during the acute stages of mdx disease (Sek et al., 2019). However, genetic inhibition of eosinophil-mediated cytotoxicity reduced fibrosis in the late stages of muscular dystrophy (Wehling-Henricks et al., 2008), consistent with the view that type II immunity and eosinophils promote fibrosis in several tissues (Gieseck et al., 2018; Nussbaum et al., 2013). Elucidating the functional complexity of muscle eosinophilia first requires a thorough understanding of how eosinophils are regulated during DMD.

Group 2 innate lymphoid cells (ILC2s) are a subset of tissue-resident lymphocytes that promote eosinophil homeostasis and tissue eosinophilia (Nussbaum et al., 2013). ILC2s lack antigen receptors (Moro et al., 2010), are activated by tissue alarmins (e.g., thymic stromal lymphopoietin (TSLP), IL-25, IL-33) (Mjösberg et al., 2012; Moro et al., 2010), and secrete IL-13 and IL-5, which stimulate M2 macrophages (Molofsky et al., 2013) and eosinophils (Nussbaum et al., 2013), respectively. ILC2s are activated by tissue injury and regulate repair by producing the growth factor amphiregulin (Monticelli et al., 2012), previously shown to support muscle regeneration (Burzyn et al., 2013). Based on these reported functions, we tested the hypothesis that ILC2s are activated in damaged muscle and promote muscle eosinophilia to regulate the pathogenesis of muscular dystrophy. Herein, we report a novel fibrogenic/adipogenic progenitor (FAP) and muscle ILC2 interaction that serves as the central node of regulation for muscle eosinophilia and transcriptional programs that promote muscle fibrosis.

RESULTS AND DISCUSSION

Eosinophils and eosinophilic factors are increased in human and mouse dystrophic muscle

We obtained human skeletal muscle biopsies from DMD patients and controls and enumerated MBP-1^{+} eosinophils in frozen cross-sections by immunohistochemistry. We found that eosinophils were elevated in DMD muscle compared to control patients (Figures 1A and 1B). Muscle eosinophils were also elevated in limb-girdle muscular dystrophy 2A (LGMD2A), a muscle disorder associated with known muscle eosinophilia (Krahn et al., 2006) (Figures S1A and S1B). Representative images of quadriceps show that DMD muscle

contains MBP-1-expressing eosinophils juxtaposed with myofibers (Figure 1A). Although sample size is low, a preliminary comparison of eosinophil numbers and age showed that they declined with disease progression but remained constant in healthy controls (Figure 1C). Adjacent cross-sections stained with hematoxylin and eosin (H&E) confirmed the absence or presence of active pathology in healthy controls or DMD and LGMD2a biopsies, respectively (Figure 1A; Figure S1C).

Prior histological studies have shown that eosinophils are elevated in 4-week-old dystrophic muscle, reaching a density of ~4,000 cells/mm^3 (Cai et al., 2000). Genetic ablation of their cytotoxic function significantly reduced the severity of fibrosis in mdx mice (Wehling-Henricks et al., 2008), indicating that rare immune cell populations significantly regulate the pathogenesis of muscular dystrophy. We also found that eosinophils were significantly elevated in mdx mice (Figures 1D and 1E), peaking at the acute stage of disease and remaining significantly elevated in mdx mice at 52 weeks (Figure 1E). Eosinophils in blood, bone marrow, gut, and lung were not altered between wild-type (WT) and mdx mice (Figure 1F), indicating that muscle eosinophilia is attributed to a muscle-intrinsic regulation. Dystrophic muscle eosinophils expressed the IL-5 receptor (IL-5R) and the eosinophil-recruiting receptor, CCR3, but not CCR1, CCR2, or CCR5 (Figure 1G) (Porter et al., 2003a). Furthermore, the relative expression of IL-5 and CCR3 ligands (CCL5, CCL7, CCL9) was elevated in dystrophic muscle (Figure 1H). Collectively, our data suggest that eosinophils represent a major cellular constituent of chronic muscle inflammation and highlight a potential role for IL-5 and/or eosinophil chemotactic factors in the regulation of muscle eosinophilia during muscular dystrophy.

ILC2s are activated in diseased muscle and are the predominant source of IL-5

We determined the cellular source of IL-5 by using mdx.Red5 mice, a reporter strain in which IL-5 expression was disrupted by inserting a tdTomato transgene in the IL-5 locus (Nussbaum et al., 2013). Flow cytometry analysis of single-cell suspensions prepared from 4-week-old WT.Red5$^{+/-}$ or mdx.Red5$^{+/-}$ hindlimb muscle revealed that IL-5 (Red5) was expressed by CD45$^+$ immune cells, which were increased in number in mdx mice (Figures 2A and 2B). CD45$^+$IL-5$^+$ cells expressed Thy1, CD127, and KLRG1 and were negative for immune cell lineage (Lin) markers, including CD11b, CD11c, CD19, T cell receptor (TCR), CD3, and NK1.1 (Figure 2A). This phenotype is indicative of ILC2s, a predominant source of IL-5 in adipose tissue (Molofsky et al., 2013) and barrier surfaces (Klein Wolterink et al., 2012; Moro et al., 2010). The vast majority of IL-5$^+$ cells were ILC2s, which were expanded in dystrophic muscle (Figure 2C; Figure S2A). A negligible fraction of Lin$^+$ cells, CD4$^+$ T cells, or CD45$^-$ populations expressed IL-5 (Figure 2C; Figure S2B). To further characterize the phenotypic nature of putative muscle ILC2s, we examined the expression of prototypical markers of ILC2s (Entwistle et al., 2020), including GATA3, CD25, CD127, KLRG1, IL17RB (IL-25 receptor), and ST2 (IL-33 receptor) in CD45$^+$Thy1$^+$Lin$^-$ cells (Figure 2D; Figure S2C). ILC2 markers were expressed on 70%–90% of WT and mdx CD45$^+$Thy1$^+$Lin$^-$ cells (Figure S2D), and the numbers of ILC2-marker$^+$ cells were elevated in mdx muscle (Figure S2E).

We next sought to determine the regulation of the three major subsets of ILCs, that is, ILC1s ($NK1.1^+$), ILC2s ($KLRG1^+$), and ILC3s ($ROR\gamma t^+$), during acute stages of muscular dystrophy (Figure 2E). The frequency and number of $CD45^+Thy1^+NK1.1^+$ (Figure 2F; Figure S2F) and $CD45^+Thy1^+Lin^-KLRG1^+$ (Figure 2G; Figure S2G) ILCs were increased in dystrophic compared to WT muscle. A negligible number of $CD45^+Thy1^+Lin^-ROR\gamma t^+$ cells were detected in dystrophic muscle (Figure 2H; Figure S2H). Because ILC2s promote eosinophil homeostasis (Nussbaum et al., 2013) and cytotoxic ILC1s can kill eosinophils (Pesce et al., 2017), we did not further investigate ILC1s and focused instead on the ILC2-mediated regulation of muscle eosinophilia. We also interrogated the chronicity of ILC2 expansion in dystrophic muscle and found that these cells were significantly increased at all ages examined and paralleled muscle eosinophilia (Figure S2I). Gut or lung ILC2s were not increased in mdx mice (Figure S2J), indicating that the elevated number of ILC2s in dystrophic muscle is not attributed to a systemic regulation. $KLRG1^+CD127^+$ ILC2s were also increased by ~10-fold in an inducible mouse model of facioscapulohumeral muscular dystrophy (Giesige et al., 2018) (Figure S2K), suggesting that the expansion of muscle ILC2s is a generalized response to muscle damage.

To further demonstrate that muscle injury activates ILC2s, we measured intracellular IL-13, a type 2 cytokine induced by activation (Price et al., 2010). The frequency and number of IL-13-producing ILC2s were increased by 2- and 10-fold, respectively, in 4-week-old mdx muscle (Figures 2I and 2J; Figure S2L). The relative expression of IL-13 was also increased in mdx muscle ILC2s (Figures 2K and 2L). These results indicate that muscle damage activates ILC2s that produce IL-5 and IL-13 and resemble IL-33-responsive natural ILC2s (Huang et al., 2015).

IL-33 is predominantly expressed by FAPs and activates muscle ILC2s

To gain insight on the signals promoting ILC2 activation and expansion during muscular dystrophy, we measured the expression levels of the known ILC2-activating cytokines, that is, IL-25, IL-33, and thymic stromal lymphopoietin (TSLP), in 4-week-old WT and mdx muscle. qRT-PCR revealed that IL-25, IL-33, and TSLP were upregulated in dystrophic muscle (Figure 3A). Analysis of the quantitation cycle (Cq) values, which are inversely related to transcript copy number, revealed that IL-33 displayed the lowest mean Cq values, indicating that it is the most abundantly expressed ILC2-activating cytokine in muscle (Figure 3B). IL-33 was also increased in the muscle of DMD patients compared to controls (Figure 3C), and a linear regression analysis revealed that the expression ($\Delta\Delta$Cq) positively correlated with age (Figure 3D).

qRT-PCR analysis of fluorescence-activated cell sorting (FACS)-isolated cells revealed that IL-33 was most abundantly expressed in FAPs (Figures 3E and 3F). Unexpectedly, transcript levels of IL-33 did not differ between WT and mdx muscle FAPs (Figure 3G). These results suggest that the increased expression of IL-33 in dystrophic muscle is attributed to the previously shown increase in FAPs in dystrophic muscle (Lemos et al., 2015). Immunofluorescent staining of 4-week-old mdx quadriceps confirmed that IL-33 protein (green) was expressed by $PDGFR\alpha^+$ cells (red) and localized in the nucleus (blue) (Figure 3H). To define the myofiber boundary, sections were also stained with anti-laminin antibody

(white) (Figure 3H). Consistent with their expression of ST2 but lack of the IL-25 receptor, recombinant IL-33 (rIL-33) expanded muscle ILC2s but IL-25 had no effect (Figure 3I). The IL-2 complex (IL-2c) also increased muscle ILC2s and further potentiated their expansion when used in combination with rIL-33 (IL-2c/IL-33, Figure 3I). Our finding that muscle ILC2s are responsive to IL-33, which was predominantly expressed by FAPs, suggests that FAPs are major activators of ILC2s during muscular dystrophy. However, the role of FAP-derived IL-33 remains to be directly examined.

ILC2s promote eosinophilia in dystrophic muscle through IL-5

Given that ILC2s regulate eosinophil homeostasis in other tissues (Nussbaum et al., 2013), we tested the hypothesis that muscle ILC2s are key promoters of eosinophils in dystrophic muscle. We first determined the spatial distribution of FAPs, ILC2s, and eosinophils, reasoning that if a FAP-ILC2 interaction promotes eosinophilia, then these three cell types should be present in a common niche. Quadriceps from 4-week-old mdx.Red5$^{+/-}$ mice were immunofluorescently labeled with antibodies specific for PDGFRα (white), Siglec-F (green) and tdTomato (red), which mark FAPs, eosinophils, and ILC2s, respectively. We found that all three cell types were in close proximity to each other, suggesting that these three cells types interact in dystrophic muscle (Figure 4A).

The mdx.YetCre13-DTA^{+} mouse lacks IL-13-producing cells, including ILC2s (Price et al., 2010), thus providing a novel model of muscular dystrophy to test the hypothesis that ILC2s promote muscle eosinophilia. We used flow cytometry to initially examine how the deletion of ILC2s influenced the cellular composition of dystrophic muscle, including satellite, stromal, and various immune cells. We confirmed that muscle ILC2s were reduced by ~85% in 4-week-old mdx.YetCre13.DTA$^{+/-}$ (DTA^{+}) mice compared to DTA$^{-/-}$ (DTA^{-}) littermates (Figures 4B and 4D; Figure S3A). The expansion of ILC2s in response to IL-2c/IL-33 was nearly abolished in DTA^{+} mice (Figures 4B and 4D). We also found a significant decrease in the frequency (Figure 4C; Figure S3B) and absolute number (Figure 4E) of muscle eosinophils. Furthermore, the IL-2c/IL-33-mediated expansion of muscle eosinophils was abrogated in mdx mice lacking ILC2s (Figures 4C and 4E). The depletion of ILC2s in mdx mice did not alter the frequency of regulatory T cells (Tregs), conventional T cells, satellite cells, or FAPs (Figures S3C–S3F). Although the frequency of macrophages was not affected, ILC2 deletion resulted in a small increase in the expression of PD-L1 and F4/80, suggesting that ILC2s marginally influence the activation of muscle macrophages (Figures S3G–S3I).

IL-13 is also expressed by multiple immune cells, including T helper (Th)2 T cells, invariant natural killer T (iNKT) cells, basophils, and mast cells (Wynn, 2003), raising the possibility that these cells may regulate muscle eosinophils in dystrophic muscle. TCRα-knockout (KO) mice lack T cells, including Th2 T cells, and iNKT cells. Thus, we examined muscle eosinophils in mdx.TCRαKO mice, and found that they were not affected when treated with or without IL-2c and IL-33 (Figure S3J). To address whether muscle basophils, eosinophils, or mast cells expressed IL-13 and are therefore subjected to deletion in mdx.YetCre13.DTA mice, we measured IL-13 levels in these cell types through intracellular staining and flow cytometry analysis. We found that basophils are not present in dystrophic muscle (Figure S3K), and muscle eosinophils and mast cells did not express IL-13 (Figures S3L–S3P) and

therefore were unlikely deleted in DTA$^+$ mice. Collectively, these results reveal a central role for ILC2s in the regulation of skeletal muscle eosinophilia.

We next tested whether ILC2s regulate the expression of IL-5 in dystrophic muscle by deleting or expanding ILC2s and then measuring IL-5 expression by qRT-PCR. IL-2c/IL-33 treatment significantly increased IL-5 in ILC2-sufficient mdx (DTA$^-$) mice compared to vehicle-treated DTA$^-$ mice, and this induction was substantially abrogated when ILC2s were deleted in DTA$^+$ mdx mice (Figure 4F). IL-5 levels were not different between DTA$^+$ and DTA$^-$ vehicle-treated mice, suggesting a compensatory increase in IL-5. In support of this interpretation, we found that mast cells produced IL-5 but did not express IL-13. Thus, mast cells are not deleted in DTA$^+$ mice, and this cellular source of IL-5 may compensate for the loss of IL-5-producing ILC2s (Figures S3M–S3P). CCR3 ligands were not substantially regulated by IL-2c/IL-33 treatment (Figure 4F), consistent with the observation that ILC2s are not the only source of CCR3 ligands (Figure S3Q).

To show that the loss of muscle eosinophils in DTA$^+$ mice is a muscle-intrinsic effect dependent on IL-5, we performed adoptive transfer assays in which quadriceps of DTA$^+$ mice were intramuscularly injected with IL-5-sufficient (IL-5$^{+/+}$) or -deficient (IL-5$^{-/-}$) ILC2s. In order to obtain a sufficient number of ILC2s for the adoptive transfer assays, we treated donor mdx or mdx.IL-5$^{-/-}$ mice with IL-2c/IL-33 and then FACS-isolated ILC2s. The adoptive transfer of IL-5-sufficient ILC2s increased muscle eosinophils, but eosinophil numbers did not differ between non-injected quads and those injected with IL-5-deficient ILC2s (Figure 4G). Collectively, these findings suggest that IL-5 promotes the survival or expansion of muscle eosinophils but ILC2-derived CCR3 ligands do not play a role in their recruitment.

ILC2s induce a transcriptional program associated with the promotion of muscle fibrosis

We examined how ILC2s regulate several pathological features of muscular dystrophy and regeneration. Because genes associated with fibrosis are upregulated during the acute stages of muscular dystrophy (Porter et al., 2003b), but fibrosis is not yet evident (Pessina et al., 2014), we first examined whether ILC2s regulate the expression of fibrosis-associated genes. qRT-PCR analysis of hamstring RNA revealed that the pro-fibrotic genes collagen 1α2 (Goldspink et al., 1994; Graham et al., 2010), arginase-1 (Wehling-Henricks et al., 2010) and MMP9 (Li et al., 2009) were upregulated by IL-2c/IL-33 treatment and their induction was impaired in mdx mice lacking ILC2s (Figures 4I–4K). The regulation of fibrosis-associated genes coincided with an ILC2-dependent increase in the expression of transforming growth factor (TGF)-β1 (Figure 4K) and SMAD4 (Figure 4L), suggesting that ILC2s promote TGF-β signaling to promote muscle fibrosis. Fibrosis-associated genes were not differentially regulated between vehicle-treated DTA$^+$ and DTA$^-$ mice, suggesting that other cell types in the dystrophic niche compensate for the loss of ILC2s similar to what was observed for the expression of IL-5. We also labeled quadriceps with collagen 1 antibodies to assess fibrosis and found no difference in the collagen$^+$ area in all the conditions that were tested (Figures S4A and S4D). This is anticipated given that fibrosis has not yet developed in mdx hindlimb muscle at the acute stages of disease (Pessina et al., 2014).

Micro-lesions in the sarcolemma owing to dystrophin deficiency cause the aberrant accumulation of serum proteins (e.g., albumin) in the cytosol of injured myofibers (Matsuda et al., 1995). Thus, to determine the effect of ILC2 deletion or expansion on muscle injury, we measured the frequency of serum albumin-positive (SA^+) myofibers and the total muscle area occupied by injured fibers. We found no difference in the injured area or frequency of injured myofibers in DTA^+ or DTA^- mice treated with IL-2c/IL-33 or vehicle (Figures S4B, S4E, and S4F). We next examined whether ILC2s regulate muscle regeneration by measuring the proportion of embryonic myosin heavy chain-positive ($eMyHC^+$) regenerating myofibers and their cross-sectional area (CSA). Although the proportion of $eMyHC^+$ regenerating myofibers was not affected by depletion or expansion of ILC2s (Figures S4C and 4G), we found an over-representation of small myofibers in mdx mice lacking ILC2s (DTA^+) compared to ILC2-sufficient mdx mice (DTA^-) (Figure S4H). However, no difference was noted between DTA^- and DTA^+ mice that were treated with IL-2c/IL-33 (Figure S4I). Given that transcriptional programs associated with fibrosis can impede muscle regeneration (Gardner et al., 2020; Mann et al., 2011), the increased proportion of small regenerating myofibers when ILC2s are depleted in mdx mice may reflect the beginning phases of an improved muscle regenerative response. Future studies will focus on performing kinetic studies by examining CSA at different ages and determining the mechanism controlling the ILC2-mediated regulation of muscle regeneration.

Prior studies have linked muscle eosinophilia with the development of muscle fibrosis (Wehling-Henricks et al., 2008), but how this link is established during muscular dystrophy is not clear. In this study, we discovered that IL-33 receptor (ST2)-expressing ILC2s reside in healthy skeletal muscle, indicating that they are constituents of the muscle-resident immune cell niche. IL-33 was increased in dystrophic muscle and expanded eosinophils in an ILC2/IL-5-dependent manner. Our observation that FAPs were the predominant source of IL-33 suggests that a ST2/IL-33 signaling axis mediates a novel FAP and ILC2 interaction that promotes muscle eosinophilia during muscular dystrophy. A Treg and stromal cell interaction mediated by IL-33 was recently reported to guide the tempo of muscle regeneration following acute injury (Kuswanto et al., 2016), questioning whether ILC2s similarly promote regeneration. Unexpectedly, we found that the expansion of ILC2s with IL-33/IL-2c induced the expression of genes associated with muscle fibrosis, suggesting that their chronic activation may promote fibrosis in muscular dystrophy. Because fibrosis requires 1.5 years to develop in the mdx hindlimb muscles (Pastoret and Sebille, 1995), and is evident in the diaphragm by 6 months of age (Stedman et al., 1991), future studies will require aging mdx.YetCre13.DTA mice beyond these ages to rigorously examine the role of ILC2s in muscle fibrosis, and how this may subsequently impair muscle regeneration.

A developing paradigm begins to emerge in which FAP-derived signals, such as IL-33, play an instrumental role in orchestrating the immune response to muscle injury. The outcome of IL-33-mediated immune responses on skeletal muscle function likely depend on the nature of the muscle insult (e.g., acute injury versus chronic muscle degeneration), as well as the immune cells targeted by IL-33 (Tregs versus ILC2s). IL-33 and IL-2c promote regeneration during acute muscle injuries through their action on muscle Tregs (Burzyn et al., 2013; Kuswanto et al., 2016). Our, findings suggest that the pro-regenerative function of IL-33 and

IL-2c are independent of ILC2s, and that in chronic disease settings ILC2s promote fibrosis. In summary, our findings contribute to this emerging paradigm by showing that ILC2s play a central role in linking stromal and innate immune responses during muscular dystrophy to induce a fibrosis-associated transcriptome. Further defining the cellular and molecular regulation of this link marks a major advancement in understanding how chronic inflammation promotes muscle fibrosis and will facilitate development of novel therapies for DMD.

STAR★METHODS

RESOURCE AVAILABILITY

Lead contact—Further information and requests for reagents or other resources should be directed to Armando Villalta (armando.villalta@uci.edu).

Materials availability—No unique materials were generated during this study.

Data and code availability—This study did not generate any unique datasets or code.

EXPERIMENTAL MODEL AND SUBJECT DETAILS

Animal studies—All animal experiments were conducted according to protocols approved by the Institutional Animal Care and Use Committee at the University of California, Irvine. All mice were housed with littermates on a 12:12 light/dark cycle and were provided food and water *ad libitum*. Mdx mice were purchased from the Jackson laboratory and bred in our colony. New mdx breeders were purchased after the 5th generation of breeding to avoid genetic drift. Mdx mice lacking ILC2s were generated by crossing mdx mice with the YetCre13 mice (Price et al., 2010) in which the endogenous IL-13 promoter drives the expression of a yellow fluorescent protein (YFP)-Cre recombinase fusion protein. Mdx.YetCre13 mice were subsequently bred with mdx that were crossed with DTA transgenic mice in which a DTA transgene carrying a flox-stop-flox cassette was knocked into the ROSA26 locus (Voehringer et al., 2008). Cre expression in IL-13-producing cells leads to the excision of the stop cassette and subsequent expression of DTA, resulting in the ablation of IL-13-producing cells in mdx mice, including ILC2s. Mdx.Red5 mice were generated by crossing mdx mice with Red5 knockin/knockout transgenic mice, in which the tdTomato transgene was inserted in the IL-5 locus, disrupting expression of endogenous IL-5 (Nussbaum et al., 2013). Mice that are heterozygous for the Red5 transgene ($Red5^{+/-}$) served as an IL-5 reporter strain in our studies that retained IL-5 expression, whereas mice that are homozygous for the Red5 transgene ($Red5^{+/+}$) are IL-5 deficient. The TIC-DUX4 mouse model of facioscapulohumeral muscular dystrophy (FSHD) was generated as previously described (Giesige et al., 2018) and provided by Dr. Scott Harper. Briefly, Rosa26-DUX4 mice (The Jackson Laboratory) were crossed with HSA-mER-CRE-mER mice (The Jackson Laboratory) to yield the TIC-DUX4 strain. To induce Cre recombinase, 16-wk-old mice were orally treated with tamoxifen (Millipore Sigma). Tamoxifen was dissolved to a 10% final volume with 95% ethanol and then diluted to a final concentration of 15 mg/ml with sunflower seed oil. TIC-DUX4 and littermate controls received two 150 mg/kg doses of tamoxifen on days 0 and 2 and were sacrificed on day 10. Unless otherwise

noted, mice used in this study were analyzed at 4 weeks of age. Genotyping primer sequences for mice used in this study are listed in Table S3.

Human studies—Deidentified frozen, muscle cross-sections from archived human muscle biopsies provided by the Muscular Dystrophy Tissue and Cell Repository at the University of Iowa, and their identity remained confidential throughout the study. Prior to biopsy collection, participants were informed about the requirements and potential risks of the procedures before providing their written informed consent in accordance with the Department of Health and Human Services regulations, 45 CFR 46. Patient information and characteristics are provided in Table S1.

METHOD DETAILS

Study approval—Human muscle biopsies were collected with written consent and approval from the University of Iowa Institutional Review Board in accordance with the Department of Health and Human Services regulations, 45 CFR 46. All animal experiments were conducted according to protocols approved by the Institutional Animal Care and Use Committee at the University of California, Irvine.

Cell isolation and flow cytometry analysis

Muscle: Single-cell suspensions from mouse hind limb muscles were prepared as previously described (Kastenschmidt et al., 2018). Briefly, mice were first euthanized with carbon dioxide using a gradual fill method per American Veterinary Medical Association guidelines and were perfused with 1X PBS. The popliteal lymph node was removed, and all hind limb muscles were excised then mechanically and enzymatically digested, filtered through 70 and 40 μm mesh filters (Genesee Scientific), and cells were purified using gradient centrifugation.

Lung: Single-cell suspensions from the lungs of mice were isolated using mechanical and enzymatic digestion. The trachea was exposed and 1 mL of digestion media composed of RPMI (Lonza) containing 0.1 mg/ml collagenase P (Roche) and 0.02 mg/ml DNase (Roche) was injected into the trachea to inflate the lungs. The lungs were then dissected and minced, and digested in 3 mL of digestion media for 45 minutes while rocking at 37°C. Following digestion, suspensions were diluted with HBSS and filtered through 70 μm filter and pelleted using centrifugation. Red blood cells were lysed by incubating cells with ACK lysis buffer (Life Technologies) for 5 minutes. Single-cell suspensions were then analyzed using flow cytometry.

Gut: Single-cell suspensions were isolated from mouse intestine by adapting a previously reported protocol (Moro et al., 2015). Mouse small intestine was excised from euthanized animals and cut longitudinally then into 3 cm pieces. Tissue was then washed in HBSS (Lonza) containing 15mM HEPES (Corning) and penicillin-streptomycin (Life Technologies) by vigorous shaking in a 50 mL conical tube, then incubated in HBSS containing 15mM HEPES, 5mM EDTA (Invitrogen) and 10% FBS (Corning) for 20 minutes while rocking. The intestines were washed in 1x PBS then digested in prewarmed IMDM (GIBCO) containing 10% FBS with 20 μg/ml liberase and 50 μg/ml DNaseI for 30 minutes

while rocking at 37°C. Following the first round of digestion, tissue was mechanically dissociated with a gentle macs dissociator (program M_intestine_01) and incubated for an additional 30 minutes at 37°C while rocking. The digested supernatant was then filtered through a 70 μm filter and remaining tissue was crushed with a syringe plunger. Cells were then filtered through a 40 μm cell strainer and pelleted by centrifugation (500xg for 5 minutes) for downstream flow cytometry analysis.

Flow cytometry—Isolated cells were stained with Zombie NIR fixable viability dye (Biolegend) for 15 minutes, and the FC receptor was blocked by incubating cells for 15 minutes in TruStain FcX anti-mouse CD16/32 antibody (Biolegend). Anti-mouse antibodies used in this study are listed in the key resources table. Lineage dumps in this study are as listed or are composed of a cocktail of antibodies specific for CD19, CD11b, CD11c, NK1.1, CD3, and TCRβ (Figures 2A, 2D, and 4) or CD19, CD11b, CD11c, CD3, and TCRβ (Figures 2E–2H). The intracellular staining of transcription factors was performed using the Foxp3/Transcription factor staining buffer set (Thermo Fisher) per manufacturer directions. Surface and intracellular stains were incubated for 30 minutes while on ice and protected from light. For the detection of intracellular IL-13 (Hirota et al., 2018), single-cell suspensions were stimulated in RPMI supplemented with 10% fetal bovine serum containing phorbol myristate acetate (50 ng/ml; Sigma) and ionomycin (500 ng/ml; Sigma) for 4 hours at 37°C. Brefeldin A (1 μg/ml; Sigma) was added to cells for the last 2 hours of stimulation and cells were washed and stained as described above. Single-cell suspensions were analyzed or isolated by fluorescence-activated cell sorting (FACS) using a FACSAria Fusion (BD Biosciences) equipped with 405, 488, 561, and 640 lasers. Data were analyzed, flow and TSNE plots were generated using FlowJo software. For data displayed as histograms, modal = normalized to mode.

***In vivo* cytokine treatment—**IL-2c was prepared by combining 0.5 mg recombinant mouse IL-2 (eBioscience) with 5 mg anti-mouse-IL-2 antibody (eBioscience) and incubated at 37°C for 15 minutes. Mice were treated with isotype control, IL-2c, 0.5 mg recombinant mouse IL-33 (Invitrogen), IL-2c in combination with IL-33, 0.5 mg recombinant mouse IL-25 (R and D systems), or IL-2c in combination with IL-25 (Price et al., 2010). Mice in all treatment groups were administered agents intraperitoneally starting at 2 weeks of age. Animals were injected every other day for a total of 3 injections and were euthanized at 4 weeks of age.

Adoptive transfer of ILC2s

Isolation of donor ILC2s: 4-wk-old mdx and mdx.Red5$^{+/+}$ (IL-5$^{-/-}$) mice were treated with IL-2c and IL-33 as described above. Mice were intraperitoneally injected three times every other day and euthanized 6 days after the initial injection. Hind limb muscles were collected then mechanically and enzymatically dissociated. Following filtration, cells were purified using gradient centrifugation. Cells suspensions were stained with Zombie NIR fixable viability dye, and FC receptors were blocked by incubating cells for 15 minutes with the CD16/32 antibody. Cell surface staining was performed for 30 minutes while on ice and protected from light using appropriate anti-mouse antibodies to isolate ILCs by fluorescence-activated cell sorting (FACS).

Adoptive transfer of ILC2s: Freshly sorted ILC2s were immediately injected into the quadriceps of mdx.YetCre.DTA+ recipient mice. Briefly, mice were anesthetized with isoflurane while placed over a heat pad to maintain thermoregulation. Anesthetized mice were sterilized with 70% ethanol. Five μl of cell suspension (5000 cells/μl in PBS) were injected into the quadriceps using a Hamilton syringe. The contralateral quadriceps was used as a non-injected control. Flow analysis of the quadriceps of mdx.Yetcre.DTA^{+} mice was performed 4 days following the adoptive transfer of ILC2s.

Examination of gene expression using quantitative qRT-PCR: Liquid nitrogen-frozen muscle samples were homogenized, and RNA was extracted using TRIsure (Bioline) and the Quick-RNA Miniprep kit (Zymo Research) per manufacturer instructions. Cell populations were sorted directly into lysis buffer, and RNA was isolated using the Quick-RNA Microprep kit (Zymo Research). Complementary DNA (cDNA) was synthesized from 150 ng (sorted cells) or 1000 ng (whole muscle) of DNase-treated RNA using the SensiFAST cDNA synthesis kit (Bioline). Gene expression was quantified using TaqMan expression assay probes (Life Technologies) and 2x SensiFAST probe No-ROX mix (Bioline). All gene expression was normalized to 18 s unless otherwise noted.

Histological analysis and quantification

Human MBP1: For the staining of human major basic protein (MBP-1), human sections were first fixed in 2% paraformaldehyde, and endogenous peroxidases were blocked with 3% H_2O_2 (v/v in 1x PBS; Sigma) for 15 minutes. Sections were also blocked using an avidin/biotin blocking kit (Vector Laboratories) per manufacturer instructions. Blocking of non-specific immunostaining was performed by incubating sections with 5% normal donkey serum and 3% bovine serum albumin (in 1X tris-buffered saline with 0.05% Tween-20 (Blocking buffer) for 1 hour. Sections were incubated with primary antibodies against human major basic protein (1:50, Bio-Rad) overnight at 4°C. Slides were then stained with biotin anti-mouse IgG (1:200, Jackson ImmunoResearch) followed by peroxidase streptavidin (1:1000, Jackson ImmunoResearch). To visually detect MBP-1 staining, sections were incubated with peroxidase substrate (AEC substrate kit, Vector Laboratories) per manufacturer instructions for 3 minutes.

For the histological analysis of mouse muscle, quadriceps were excised, frozen in liquid nitrogen-cooled isopentane and stored at −80°C. Eight-micron cross-sections were prepared on a Leica CM1950 cryostat, mounted on positively charged microscope slides (Fisher) and stored at −80°C until the time of staining. Slides were then fixed in 2% paraformaldehyde for 10 minutes, washed in 1X PBS for 5 minutes and incubated for 1 hour in blocking buffer. Sections were then stained with primary and secondary antibodies as described:

Laminin, IL-33, Serum Albumin, Collagen, DsRed, and Siglec-F: Following blocking, sections were incubated with primary antibodies against laminin (1:200, Sigma), serum albumin (1:300, R&D systems), collagen (1:500, R&D systems), IL-33 (1:200, R&D systems) and siglec-F (1:200, BD Biosciences) diluted in blocking buffer at RT. To detect the tdTomato in Red5 mice, mice were incubated with antibodies against DsRed (1:200,

Takara) for 3 hours at RT. Cross-sections were then washed in 1X PBS and incubated with corresponding secondary antibodies to detect the antigen of interest.

PDGFRα: For the immunofluorescence staining of PDGFRα (Figure 3H), slides were blocked with 3% H_2O_2 for 15 minutes following fixation to inhibit endogenous peroxidases. Sections were the blocked for 1 hour with blocking buffer at RT. Tissues were incubated with primary antibodies against PDGFRα (1:300, eBioscience) for 3 hours, washed with 1X PBS, and stained with secondary antibodies for 3 hours (1:200) A Tyramide SuperBoost kit (Invitrogen) was used for the detection of PDGFRα per manufacturer instructions. For PDGFRα staining in Figure 4A, sections were stained with antibodies against PDGFRα (1:200, R and D systems) diluted in blocking buffer for 3 hours at RT, followed by staining with corresponding secondary antibody for 1 hour at RT.

eMyHC: Following fixation, endogenous biotin was blocked with an avidin/biotin blocking kit (Vector Laboratories) per manufacturer instructions. Following washes with 1X PBS, endogenous mouse IgG was blocked with mouse-on-mouse blocking reagent (Vector laboratories) for 1 hour at RT. Muscle sections were washed in 1X PBS and incubated for 5 minutes at RT in blocking buffer. Primary antibodies against mouse eMyHC (1:30) were diluted in blocking buffer and were incubated with sections for 1 hour at RT. To detect eMyHC labeling, sections were incubated with biotinylated anti-mouse antibodies (1:80 dilution) for 10 min followed by labeling with Alexa 594-conjugated streptavidin (1:62.5 dilution) for 5 minutes.

After incubation with primary and secondary antibodies as described, sections were counter-stained with 4′,6-diamidino-2-phenylindole, dihydrochloride (DAPI, Sigma, 1.2 nM in 1X PBS) for 10 min to visualize nuclei. Following staining, all sections were mounted with a coverslip and were imaged on a Keyence BZ-X700 inverted microscope (Keyence). All images were saved as high-quality TIFF files for downstream use. To quantify MBP-1^+ eosinophils, all cells positive for MBP-1 in the entire muscle cross-section were manually counted using FIJI. The number of cells was normalized to the section area (mm^2). To measure the collagen 1α1 and serum albumin positive area (percent of total area), the entire muscle cross section was measured in FIJI. The collagen or serum albumin image was then thresholded to define the positive pixels. The percent area positive for collagen or serum albumin was calculated using the “Area Fraction” measurement.

The percent of eMyHC- and SA- positive cells were measured using the muscle analysis software, QuantiMus, and its associated pipeline as previously described (Kastenschmidt et al., 2019). Briefly, laminin-stained images of entire muscle quadriceps were loaded into the QuantiMus software to generate a binary image. QuanitiMus’ machine learning algorithms were used to accurately define and classify each myofiber. Single-channel images of eMyHC- and SA-stained cross-sections were overlaid onto the classified image, and thresholded to define the positive fibers. The percent of total fibers positive was defined as the number of eMyHC- or SA-positive fibers divided by the total number of fibers detected and multiplied by 100%.

QUANTIFICATION AND STATISTICAL ANALYSIS

Statistical parameters including the exact value of n and statistical significance are reported in the figures and their associated legends. Results were analyzed using an unpaired t test with Welch's correction or a one-way ANOVA with Bonferroni correction where indicated. Calculations were performed in Graphpad prism. Asterisks indicate statistical significance (*, $p < 0.05$; **, $p < 0.01$; ***, $p < 0.001$, ****, $p < 0.0001$). Data displayed as bar graphs represents the mean ± SEM. Lines in scatterplots represent the mean of the data.

Supplementary Material

Refer to Web version on PubMed Central for supplementary material.

ACKNOWLEDGMENTS

This work was supported by NIH grants R21AI134567 and KL2TR001416 and an ICTS-UCI pilot award (to S.A.V.); P50AR070604, P50HD060848, R01AR062123, and Muscular Dystrophy Association grant 418933 (to S.Q.H.); UL1TR001414 (to T.M.); T32AI060573 (to J.M.K.); W81XWH1910012 (to G.C.); and TL1TR001069 (to C.R.G.). S.A.V. and R.M.L. were supported by HHMI. We also thank the Wellstone Muscular Dystrophy Cooperative Research Center at the University of Iowa for providing de-identified muscle cross-sections.

REFERENCES

Burzyn D, Kuswanto W, Kolodin D, Shadrach JL, Cerletti M, Jang Y, Sefik E, Tan TG, Wagers AJ, Benoist C, and Mathis D (2013). A special population of regulatory T cells potentiates muscle repair. Cell 155, 1282–1295. [PubMed: 24315098]

Cai B, Spencer MJ, Nakamura G, Tseng-Ong L, and Tidball JG (2000). Eosinophilia of dystrophin-deficient muscle is promoted by perforin-mediated cytotoxicity by T cell effectors. Am. J. Pathol. 156, 1789–1796. [PubMed: 10793090]

Entwistle LJ, Gregory LG, Oliver RA, Branchett WJ, Puttur F, and Lloyd CM (2020). Pulmonary group 2 innate lymphoid cell phenotype is context specific: Determining the effect of strain, location, and stimuli. Front. Immunol. 10, 3114. [PubMed: 32038635]

Gardner T, Kenter K, and Li Y (2020). Fibrosis following acute skeletal muscle injury: Mitigation and reversal potential in the clinic. J. Sports Med. (Hindawi Publ. Corp.) 2020, 7059057.

Gieseck RL 3rd, Wilson MS, and Wynn TA (2018). Type 2 immunity in tissue repair and fibrosis. Nat. Rev. Immunol. 18, 62–76. [PubMed: 28853443]

Giesige CR, Wallace LM, Heller KN, Eidahl JO, Saad NY, Fowler AM, Pyne NK, Al-Kharsan M, Rashnonejad A, Chermahini GA, et al. (2018). AAV-mediated follistatin gene therapy improves functional outcomes in the TIC-DUX4 mouse model of FSHD. JCI Insight 3, e123538.

Goldspink G, Fernandes K, Williams PE, and Wells DJ (1994). Age-related changes in collagen gene expression in the muscles of *mdx* dystrophic and normal mice. Neuromuscul. Disord. 4, 183–191. [PubMed: 7919967]

Graham KM, Singh R, Millman G, Malnassy G, Gatti F, Bruemmer K, Stefanski C, Curtis H, Sesti J, and Carlson CG (2010). Excessive collagen accumulation in dystrophic (mdx) respiratory musculature is independent of enhanced activation of the NF-κB pathway. J. Neurol. Sci. 294, 43–50. [PubMed: 20471037]

Heredia JE, Mukundan L, Chen FM, Mueller AA, Deo RC, Locksley RM, Rando TA, and Chawla A (2013). Type 2 innate signals stimulate fibro/adipogenic progenitors to facilitate muscle regeneration. Cell 153, 376–388. [PubMed: 23582327]

Hirota K, Hashimoto M, Ito Y, Matsuura M, Ito H, Tanaka M, Watanabe H, Kondoh G, Tanaka A, Yasuda K, et al. (2018). Autoimmune Th17 cells induced synovial stromal and innate lymphoid cell secretion of the cytokine GM-CSF to initiate and augment autoimmune arthritis. Immunity 48, 1220–1232.e5. [PubMed: 29802020]

Hoffman EP, Brown RH Jr., and Kunkel LM (1987). Dystrophin: The protein product of the Duchenne muscular dystrophy locus. Cell 51, 919–928. [PubMed: 3319190]

Huang Y, Guo L, Qiu J, Chen X, Hu-Li J, Siebenlist U, Williamson PR, Urban JF Jr., and Paul WE (2015). IL-25-responsive, lineage-negative KLRG1(hi) cells are multipotential 'inflammatory' type 2 innate lymphoid cells. Nat. Immunol. 16, 161–169. [PubMed: 25531830]

Kastenschmidt JM, Avetyan I, and Armando Villalta S (2018). Characterization of the inflammatory response in dystrophic muscle using flow cytometry. In Duchenne Muscular Dystrophy: Methods and Protocols, Bernardini C, ed. (Springer), pp. 43–56.

Kastenschmidt JM, Ellefsen KL, Mannaa AH, Giebel JJ, Yahia R, Ayer RE, Pham P, Rios R, Vetrone SA, Mozaffar T, and Villalta SA (2019). QuantiMus: A machine learning-based approach for high precision analysis of skeletal muscle morphology. Front. Physiol. 10, 1416. [PubMed: 31849692]

Klein Wolterink RG, Kleinjan A, van Nimwegen M, Bergen I, de Bruijn M, Levani Y, and Hendriks RW (2012). Pulmonary innate lymphoid cells are major producers of IL-5 and IL-13 in murine models of allergic asthma. Eur. J. Immunol. 42, 1106–1116. [PubMed: 22539286]

Krahn M, Lopez de Munain A, Streichenberger N, Bernard R, Pécheux C, Testard H, Pena-Segura JL, Yoldi E, Cabello A, Romero NB, et al. (2006). *CAPN3* mutations in patients with idiopathic eosinophilic myositis. Ann. Neurol. 59, 905–911. [PubMed: 16607617]

Kuswanto W, Burzyn D, Panduro M, Wang KK, Jang YC, Wagers AJ, Benoist C, and Mathis D (2016). Poor repair of skeletal muscle in aging mice reflects a defect in local, interleukin-33-dependent accumulation of regulatory T cells. Immunity 44, 355–367. [PubMed: 26872699]

Lemos DR, Babaeijandaghi F, Low M, Chang CK, Lee ST, Fiore D, Zhang RH, Natarajan A, Nedospasov SA, and Rossi FMV (2015). Nilotinib reduces muscle fibrosis in chronic muscle injury by promoting TNF-mediated apoptosis of fibro/adipogenic progenitors. Nat. Med. 21, 786–794. [PubMed: 26053624]

Li H, Mittal A, Makonchuk DY, Bhatnagar S, and Kumar A (2009). Matrix metalloproteinase-9 inhibition ameliorates pathogenesis and improves skeletal muscle regeneration in muscular dystrophy. Hum. Mol. Genet. 18, 2584–2598. [PubMed: 19401296]

Mann CJ, Perdiguero E, Kharraz Y, Aguilar S, Pessina P, Serrano AL, and Muñoz-Cánoves P (2011). Aberrant repair and fibrosis development in skeletal muscle. Skelet. Muscle 1, 21. [PubMed: 21798099]

Matsuda R, Nishikawa A, and Tanaka H (1995). Visualization of dystrophic muscle fibers in mdx mouse by vital staining with Evans blue: Evidence of apoptosis in dystrophin-deficient muscle. J. Biochem. 118, 959–964. [PubMed: 8749313]

Mjösberg J, Bernink J, Golebski K, Karrich JJ, Peters CP, Blom B, te Velde AA, Fokkens WJ, van Drunen CM, and Spits H (2012). The transcription factor GATA3 is essential for the function of human type 2 innate lymphoid cells. Immunity 37, 649–659. [PubMed: 23063330]

Molofsky AB, Nussbaum JC, Liang H-E, Van Dyken SJ, Cheng LE, Mohapatra A, Chawla A, and Locksley RM (2013). Innate lymphoid type 2 cells sustain visceral adipose tissue eosinophils and alternatively activated macrophages. J. Exp. Med. 210, 535–549. [PubMed: 23420878]

Monticelli LA, Sonnenberg GF, Abt MC, Alenghat T, Ziegler CGK, Doering TA, Angelosanto JM, Laidlaw BJ, Yang CY, Sathaliyawala T, et al. (2012). Innate lymphoid cells promote lung-tissue homeostasis after infection with influenza virus. Nat. Immunol. 12, 1045–1054.

Moro K, Yamada T, Tanabe M, Takeuchi T, Ikawa T, Kawamoto H, Furusawa J, Ohtani M, Fujii H, and Koyasu S (2010). Innate production of T_H2 cytokines by adipose tissue-associated c-Kit $^+$Sca-1$^+$ lymphoid cells. Nature 463, 540–544. [PubMed: 20023630]

Moro K, Ealey KN, Kabata H, and Koyasu S (2015). Isolation and analysis of group 2 innate lymphoid cells in mice. Nat. Protoc. 10, 792–806. [PubMed: 25927389]

Nussbaum JC, Van Dyken SJ, von Moltke J, Cheng LE, Mohapatra A, Molofsky AB, Thornton EE, Krummel MF, Chawla A, Liang H-EE, and Locksley RM (2013). Type 2 innate lymphoid cells control eosinophil homeostasis. Nature 502, 245–248. [PubMed: 24037376]

Pastoret C, and Sebille A (1995). *mdx* mice show progressive weakness and muscle deterioration with age. J. Neurol. Sci. 129, 97–105. [PubMed: 7608742]

Pesce S, Thoren FB, Cantoni C, Prato C, Moretta L, Moretta A, and Marcenaro E (2017). The innate immune cross talk between NK cells and eosinophils is regulated by the interaction of natural

cytotoxicity receptors with eosinophil surface ligands. Front. Immunol. 8, 510. [PubMed: 28503177]

Pessina P, Cabrera D, Morales MG, Riquelme CA, Gutiérrez J, Serrano AL, Brandan E, and Muñoz-Cánoves P (2014). Novel and optimized strategies for inducing fibrosis in vivo: focus on Duchenne muscular dystrophy. Skelet. Muscle 4, 7. [PubMed: 25157321]

Porter JD, Guo W, Merriam AP, Khanna S, Cheng G, Zhou X, Andrade FH, Richmonds C, and Kaminski HJ (2003a). Persistent overexpression of specific CC class chemokines correlates with macrophage and T-cell recruitment in mdx skeletal muscle. Neuromuscul. Disord. 13, 223–235. [PubMed: 12609504]

Porter JD, Merriam AP, Leahy P, Gong B, and Khanna S (2003b). Dissection of temporal gene expression signatures of affected and spared muscle groups in dystrophin-deficient (mdx) mice. Hum. Mol. Genet. 12, 1813–1821. [PubMed: 12874102]

Price AE, Liang HE, Sullivan BM, Reinhardt RL, Eisley CJ, Erle DJ, and Locksley RM (2010). Systemically dispersed innate IL-13-expressing cells in type 2 immunity. Proc. Natl. Acad. Sci. USA 107, 11489–11494. [PubMed: 20534524]

Schindelin J, Arganda-Carreras I, Frise E, Kaynig V, Longair M, Pietzsch T, Preibisch S, Rueden C, Saalfeld S, Schmid B, et al. (2012). Fiji: An open-source platform for biological-image analysis. Nat. Methods 9, 676–682. [PubMed: 22743772]

Sek AC, Moore IN, Smelkinson MG, Pak K, Minai M, Smith R, Ma M, Percopo CM, and Rosenberg HF (2019). Eosinophils do not drive acute muscle pathology in the mdx mouse model of Duchenne muscular dystrophy. J. Immunol. 203, 476–484. [PubMed: 31142604]

Stedman HH, Sweeney HL, Shrager JB, Maguire HC, Panettieri RA, Petrof B, Narusawa M, Leferovich JM, Sladky JT, and Kelly AM (1991). The mdx mouse diaphragm reproduces the degenerative changes of Duchenne muscular dystrophy. Nature 352, 536–539. [PubMed: 1865908]

Villalta SA, Rosenberg AS, and Bluestone JA (2015). The immune system in Duchenne muscular dystrophy: Friend or foe. Rare Dis. 3, e1010966. [PubMed: 26481612]

Voehringer D, Liang H-E, and Locksley RM (2008). Homeostasis and effector function of lymphopenia-induced “memory-like” T cells in constitutively T cell-depleted mice. J. Immunol. 180, 4742–4753. [PubMed: 18354198]

Wehling-Henricks M, Sokolow S, Lee JJ, Myung KH, Villalta SA, and Tidball JG (2008). Major basic protein-1 promotes fibrosis of dystrophic muscle and attenuates the cellular immune response in muscular dystrophy. Hum. Mol. Genet. 17, 2280–2292. [PubMed: 18430716]

Wehling-Henricks M, Jordan MC, Gotoh T, Grody WW, Roos KP, and Tidball JG (2010). Arginine metabolism by macrophages promotes cardiac and muscle fibrosis in mdx muscular dystrophy. PLoS ONE 5, e10763. [PubMed: 20505827]

Wynn TA (2003). IL-13 effector functions. Annu. Rev. Immunol. 21, 425–456. [PubMed: 12615888]

Highlights

- Muscle ILC2s are activated and increased in diseased muscle
- IL-33 is predominantly expressed by FAPs and expands muscle ILC2s
- ILC2s drive muscle eosinophilia in an IL-5-dependent manner
- Expansion of ILC2s promotes transcription of genes associated with muscle fibrosis

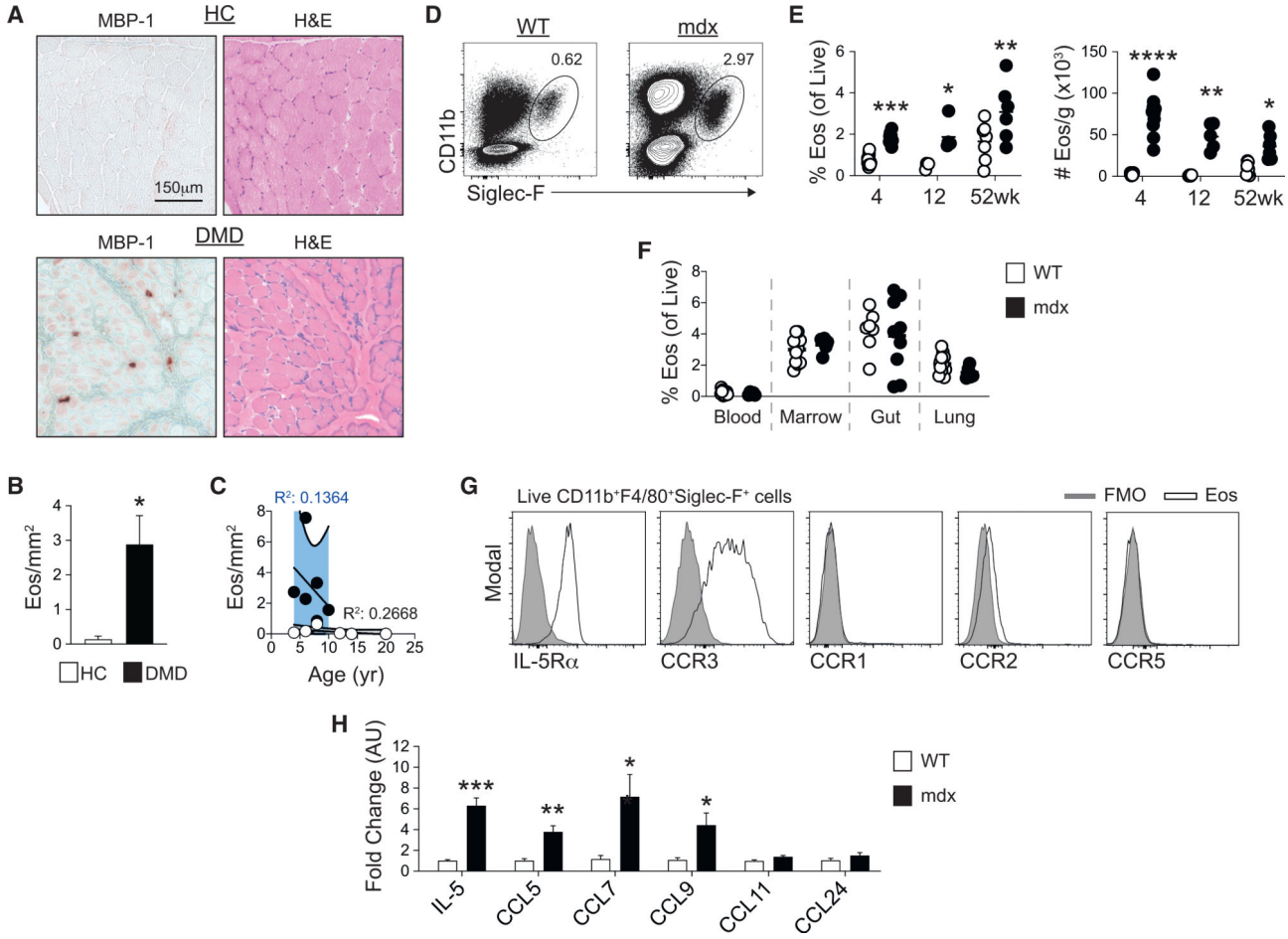

Figure 1. Eosinophilia in human and mouse dystrophic muscle

(A) Representative images of immunohistochemical staining for MBP-1 and adjacent human muscle cross-sections stained with H&E.

(B) The number of MBP-1$^+$ eosinophils (Eos) in muscle biopsies from healthy control (HC) and DMD patients. n = 6–8.

(C) Linear regression analysis of (B). HC, gray; DMD, blue.

(D) Concatenated contour plots showing live CD11b$^+$Siglec-F$^+$ Eos in WT and mdx muscle.

(E) The frequency and number of Eos in hindlimb muscle of WT and mdx mice. n = 4–16.

(F) The frequency of Eos in various tissue compartments of WT and mdx mice. n = 7–12.

(G) Representative histograms showing the expression of IL-5 and chemokine receptors on mdx muscle Eos. FMO, fluorescence minus one. n = 5.

(H) The expression of IL-5 and CCR3 ligands determined by qRT-PCR. n = 6. AU, arbitrary units.

All mice were analyzed at 4 weeks of age unless otherwise noted. *p < 0.05, **p < 0.01, ***p < 0.001, ****p < 0.0001 using an unpaired Welch's t test or one-way ANOVA with Bonferroni correction (E). Error bars indicate standard error of the mean (SEM).

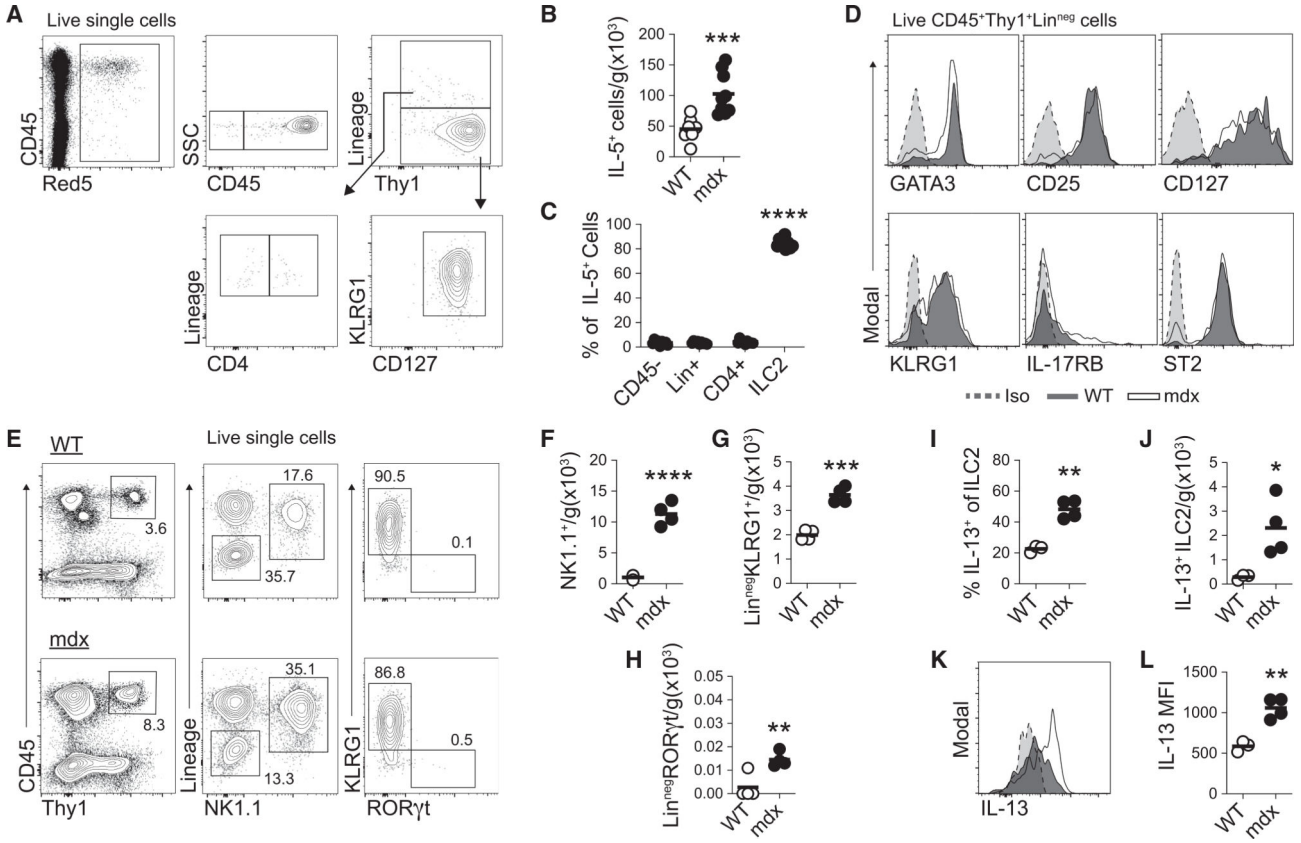

Figure 2. ILC2s are the predominant source of IL-5 in dystrophic muscle

(A) Gating strategy used to interrogate IL-5 (Red5)-expressing cells in mdx muscle.

(B) Quantification of muscle IL-5$^+$ cells using flow cytometry. n = 7–9.

(C) Percent of stroma (CD45$^-$), Lin$^+$ (Lin$^+$CD4$^-$), CD4$^+$ (Lin$^+$CD4$^+$), and ILC2s (Lin$^-$Thy1$^+$KLRG1$^+$CD127$^+$) that express IL-5 in mdx muscle. n = 9. Statistics are compared to CD45$^-$.

(D) Representative histograms showing the expression of common ILC2 markers on muscle CD45$^+$Thy1$^+$Lin$^-$ cells in WT and mdx mice. Iso, isotype control. n = 5–6.

(E) Gating strategy used to interrogate muscle ILCs.

(F–H) The number of muscle CD45$^+$Thy1$^+$NK1.1$^+$ (F), CD45$^+$Thy1$^+$Lin$^-$KLRG1$^+$ (G), and CD45$^+$Thy1$^+$Lin$^-$RORγt$^+$ (H) cells. n = 4.

(I and J) The frequency (I) and number (J) of IL-13$^+$ muscle ILC2s.

(K and L) Representative histogram (K) and the average geometric mean fluorescence intensity (MFI) (L) of IL-13 expression in CD45$^+$Thy1$^+$Lin$^-$KLRG1$^+$ muscle ILC2s.

n = 3–4 (I–L). 4-wk-old mice were analyzed. *p < 0.05, **p < 0.01, ***p < 0.001, ****p < 0.0001 using an unpaired Welch's t test (B, F–H, I, J, and L) or one-way ANOVA with Bonferroni correction (C).

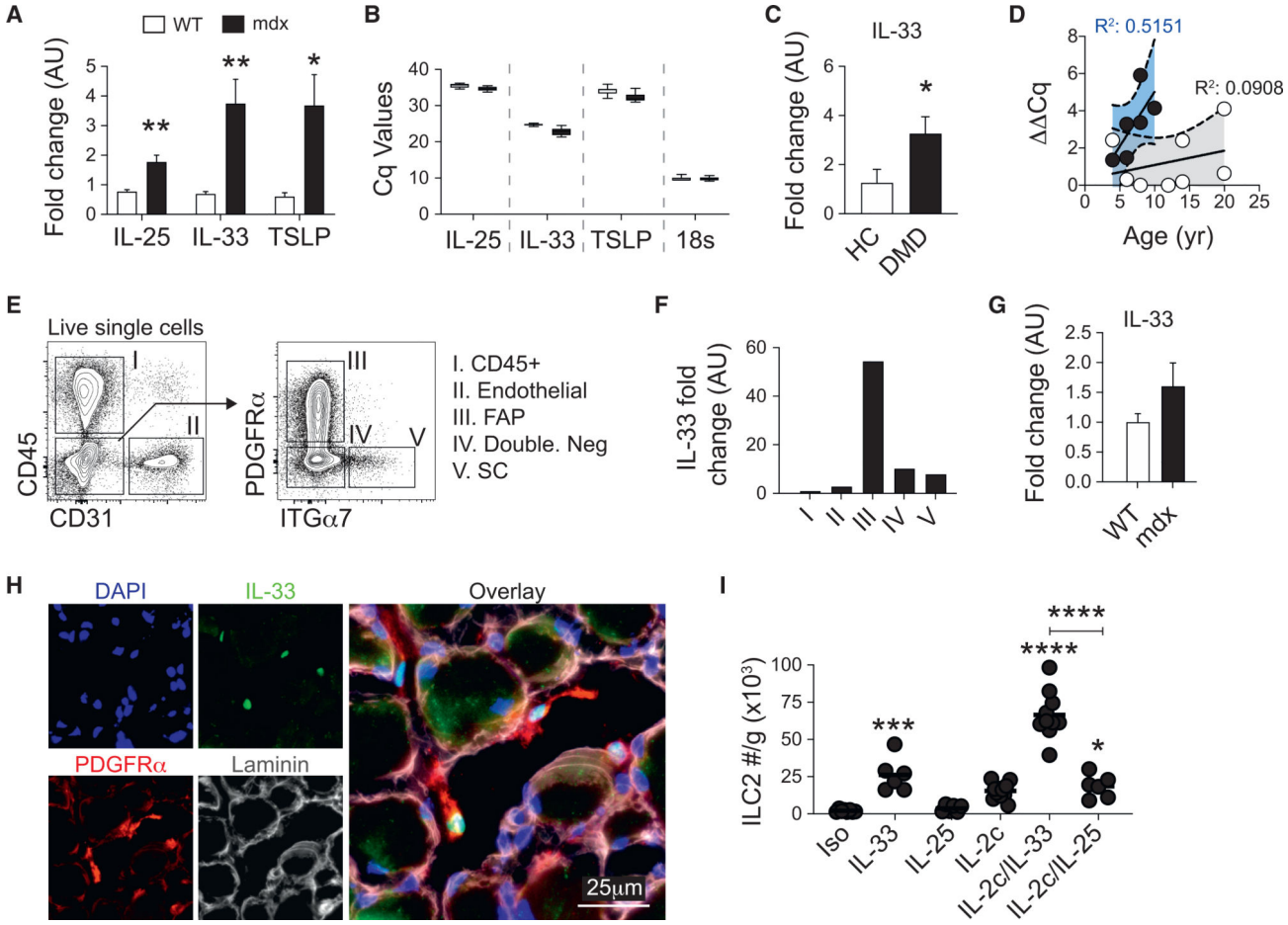

Figure 3. FAPs are the major source of IL-33, which activates muscle ILC2s

(A and B) The expression (A) and quantification cycle (Cq) values (B) of ILC2 activators in WT and mdx hamstring determined by qRT-PCR. n = 8–10.

(C) Expression of human IL-33 (hIL-33) in HC and DMD muscle biopsies. n = 6–8.

(D) Linear regression analysis comparing ΔΔCq and patient age. HC, gray; DMD, blue. n = 6–8.

(E) Gating strategy used to sort $CD45^+$ immune cells (I), $CD31^+$ endothelial cells (II), $PDGFR\alpha^+$ FAPs (III), $ITG\alpha7^+$ satellite cells (V), and $PDGFR\alpha^-$ and $ITG\alpha7^-$ double-negative (IV) cells from mdx skeletal muscle.

(F) Quantification of IL-33 expression by qRT-PCR of cell populations sorted in (E). n = 5 pooled mice.

(G) Expression of IL-33 in WT and mdx FAPs isolated by FACS. n = 4.

(H) Immunofluorescence staining of mdx quadriceps showing PDGFRα, laminin, and IL-33 expression. Nuclei were stained with DAPI.

(I) The number of muscle ILC2s in mdx mice treated with exogenous cytokines. n = 6–11. IL-2c, IL-2 complex; IL-2c/IL-33, IL-2c + IL-33; IL-2c/IL-25, IL-2c + IL-25.

*p < 0.05, **p < 0.01, ***p < 0.001, ****p < 0.0001 using an unpaired Welch's t test (A and B) or one-way ANOVA with Bonferroni correction (F). All mice were analyzed at 4 weeks of age. Error bars indicate SEM.

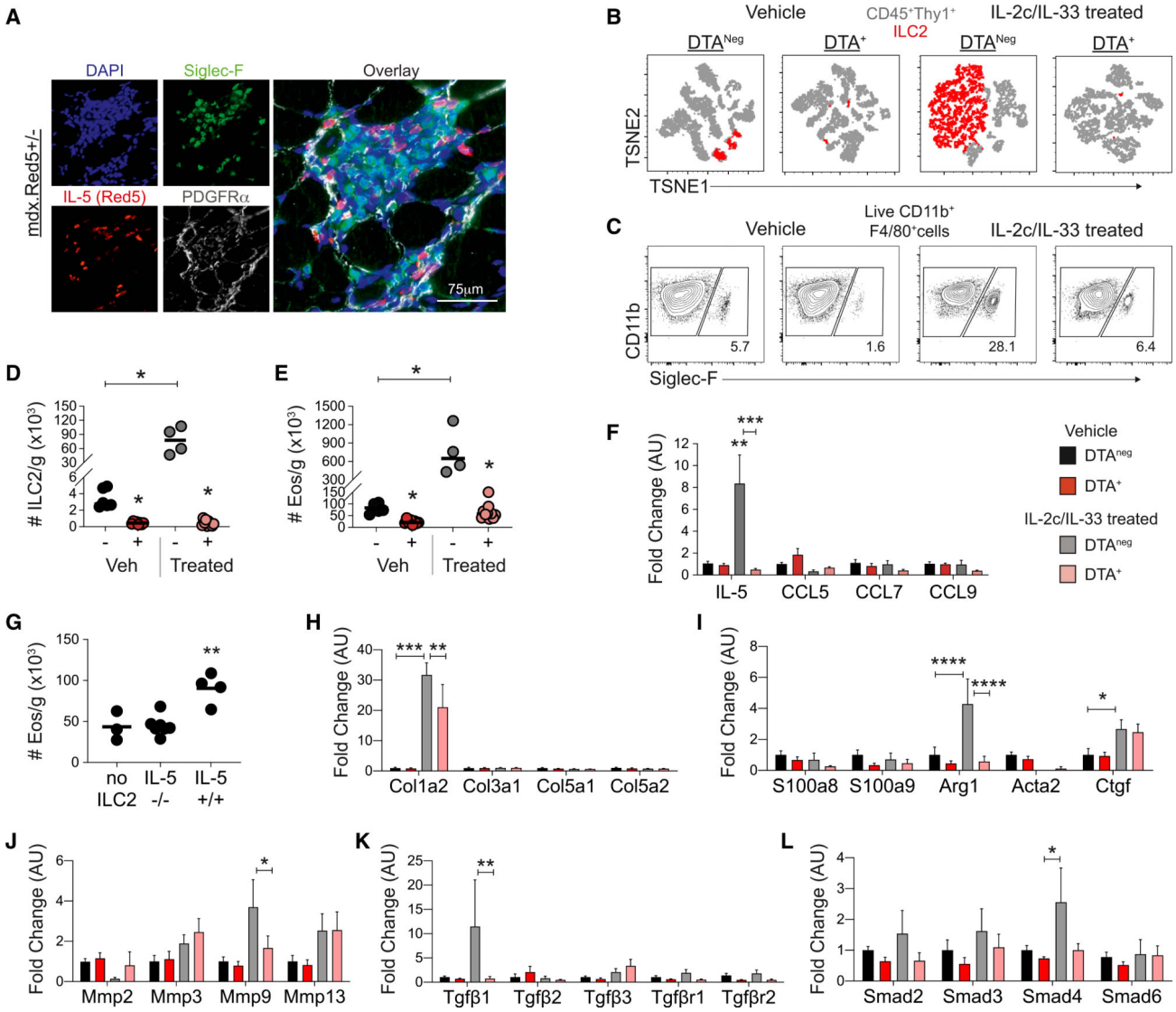

Figure 4. ILC2s promote skeletal muscle eosinophilia

(A) Immunofluorescence staining of mdx quadriceps showing IL-5 (Red5), Siglec-F, DAPI, and IL-33 expression. Nuclei were stained with DAPI.

(B) Concatenated TSNE flow plots of live $CD45^+Thy1^+$ muscle cells from DTA^- and DTA^+ mice. Grey indicates $CD45^+Thy1^+$ cells; red indicates $CD45^+Thy1^+Lin^-KLRG1^+$ ILC2s.

(C) Representative contour plots showing mdx muscle Eos ($F4/80^+CD11b^+Siglec\text{-}F^+$). Same samples used in (B).

(D and E) Quantification of flow cytometry data in (B) and (C), showing the number of ILC2s (D) and Eos (E) in vehicle (Veh)- and IL-2c/IL-33-treated (Treated) DTA^- (−) and DTA^+ (+) mice. n = 3–10.

(F) Expression of eosinophilia-promoting factors in muscle of DTA^- and DTA^+ mice treated with vehicle or IL-2c/IL-33. n = 4–8.

(G) Number of Eos detected by flow cytometry in the quadriceps of DTA^+ mice following adoptive transfer of $IL\text{-}5^{-/-}$ and $IL\text{-}5^{+/+}$ ILC2s. No ILC2 indicates non-injected muscle.

(H–L) Expression of fibrotic factors in hamstring muscle of DTA^- and DTA^+ mice treated vehicle or IL-2c/IL-33. n = 4.

*p < 0.05, **p < 0.01, ***p < 0.001, ****p < 0.0001 using an unpaired Welch's t test (D and E) or one-way ANOVA with Bonferroni correction (F–L). All mice were analyzed at 4 weeks of age. Error bars indicate SEM.

KEY RESOURCES TABLE

REAGENT or RESOURCE	SOURCE	IDENTIFIER
Antibodies		
TruStain FcX anti-mouse CD16/32 antibody	Biolegend	Cat #101302
Anti-mouse IL-5Rα (DIH37) APC	Biolegend	Cat# 153405
Anti-mouse CCR1 (S15040E) PE	Biolegend	Cat# 152507
Anti-mouse CCR3 (J073E5) APC-Fire750	Biolegend	Cat# 144521
Anti-mouse CCR5 (HM-CCR5) A488	Biolegend	Cat# 107008
Anti-mouse CCR2 (SA203G11) BV605	Biolegend	Cat# 150615
Anti-mouse CD90.2 (Thy1;30-H12) PerCP	Biolegend	Cat# 105322
Anti-mouse KLRG1 (2F/KLRG1) FITC	Biolegend	Cat# 138410
Anti-mouse CD45 (30-F11) APC	Biolegend	Cat# 103112
Anti-mouse CD4 (RM4–5) BV605	Biolegend	Cat# 100548
Anti-mouse ST2 (DIH9) PE	Biolegend	Cat# 145303
Anti-mouse IL17RB (9B10) PE	Biolegend	Cat# 146305
Anti-mouse CD25 (PC61) PE-Cy7	Biolegend	Cat# 102016
Anti-mouse NK1.1 (PK136) BV605	Biolegend	Cat# 108739
Anti-mouse CD11b (M1/70) PerCP-Cy5.5	Biolegend	Cat# 101228
Anti-mouse F4/80 (BMS) PE	Biolegend	Cat# 123110
Anti-mouse CD127 (A7R34) PE-Cy7	eBioscience	Cat #25–1271-82
Anti-mouse CD19 (eBio1D3) eFluor 450	eBioscience	Cat # 48–0193-82
Anti-mouse CD11b (M1/70) eFluor 450	eBioscience	Cat #48–0112-82
Anti-mouse CD11c (N418) eFluor 450	eBioscience	Cat #48–0114-82
Anti-mouse NK1.1 (PK136) eFluor 450	eBioscience	Cat # 48–5941-82
Anti-mouse NK1.1 (PK136) BV605	Biolegend	Cat# 103039
Anti-mouse CD3 (17A2) eFluor 450	eBioscience	Cat # 48–0032-82
Anti-mouse TCRβ (H57–597) eFluor 450	eBioscience	Cat # 48–5961-82
Anti-mouse GATA3 (TWAJ) PE	eBioscience	Cat# 12–9966-41
Anti-mouse RORγT (B2D) PE	eBioscience	Cat# 12–6981-82
Anti-mouse IL-13 (eBio13A) PE	eBioscience	Cat # 25–7133-80
Anti-mouse Siglec-F (E50–2440) BV421	BD Biosciences	Cat # 562681
Anti-mouse CD11b (M1/70) PerCP-Cy5.5	Biolegend	Cat# 101228
Anti-mouse F4/80 (BM8) PE	Biolegend	Cat# 123110
Anti-mouse CD45 (30-F11) FITC	eBioscience	Cat # 11–0451-81
Anti-mouse CD31 (390) BV421	Biolegend	Cat# 102423
Anti-mouse ITGα7 (334908) PE	R and D systems	Cat # FAB3518P
Anti-mouse CD140a (PDGFRα; APA5) APC	Biolegend	Cat# 135908
Anti-mouse CD117/c-Kit (2B8) APC	Biolegend	Cat# 105811
Anti-mouse FCεRI (MAR-1) FITC	Biolegend	Cat# 134305
Anti-mouse CD11b (M1/80) BV605	Biolegend	Cat# 101237

REAGENT or RESOURCE	SOURCE	IDENTIFIER
Anti-mouse CD11c (N418) BV605	Biolegend	Cat # 117333
Anti-mouse F4/80 (BM8) BV605	Biolegend	Cat# 123133
Anti-mouse KLRG1 (MAFA) BV605	Biolegend	Cat# 138419
Anti-mouse Ly6G (1A8) BV605	Biolegend	Cat# 127639
Anti-mouse CD45 (30-F11) Pac-Blue	Biolegend	Cat# 103126
Anti-mouse IL-2 (JES6–1A12)	eBioscience	Cat# 16–7022-85
Mouse anti-human MBP (BMK-13)	Bio-Rad	Cat # MCA5751
Goat anti-mouse PDGFRα (Polyclonal)	R and D systems	Cat# AF1062
Rat anti-mouse PDGFRα (APA5)	eBioscience	Cat# 14–1401-81
Goat anti-mouse IL-33 (Polyclonal)	R and D systems	Cat # AF3626
Rabbit anti-Laminin (Polyclonal)	Sigma	Cat # L-9393
Rat anti-mouse Siglec-F (E50–2440)	BD Biosciences	Cat #552125
Sheep anti-Collagen I (Polyclonal)	R and D systems	Cat # AF6220
Goat anti-mouse Serum Albumin (Polyclonal)	R and D systems	Cat # AF3329
Mouse anti-mouse eMyHC (F.1652)	DSHB	Cat # F.1652 supernatant
Rabbit anti-DsRed (Polyclonal)	Takara	Cat # 632496
Biotin anti-Mouse IgG	Jackson Immuno Research	Cat# 715–065-151
Anti-rat peroxidase streptavidin	Jackson Immuno Research	Cat# 712–035-153
Anti-goat Alexa Fluor 488	Invitrogen	Cat# A-11055
Anti-sheep Alex Fluor 594	Invitrogen	Cat# A-11016
Anti-rabbit Alexa Fluor 647	Invitrogen	Cat# A-31573
Anti-goat Alexa Fluor 647	Invitrogen	Cat# A-21469
Biotin-SP (long spacer) AffiniPure Donkey Anti-Mouse IgG (H+L)	Jackson Immuno Research	Cat# 715–065-151
Biological samples		
Human muscle biopsies	Wellstone Muscular Dystroph Research Network	https://wellstonemdcenters.nih.gov/
Chemicals, peptides, and recombinant proteins		
Zombie NIR fixable viability dye	Biolegend	Cat # 423105
Recombinant mouse IL-2	eBioscience	Cat #34–8021-82
Recombinant mouse IL-33	Invitrogen	Cat # PMC4044
Recombinant mouse IL-25	R and D systems	Cat# 13399-IL-025
Recombinant mouse IL-7	R and D systems	Cat # 407-ML 5mg
TRISure	Bioline	Cat # BIO-38032
DMEM	GIBCO	Cat # 10–569-044
FBS (Fetal Bovine Serum)	Corning	Cat # 35–011-CV
Dnase I	Roche	Cat# 10104159001
Collagenase P	Roche	Cat# 11249002001
EDTA	Invitrogen	Cat# 15575020
BSA (Bovine serum albumin)	Fisher Scientific	Cat# BP-1600–1
70 μm filter	Genesee Scientific	Cat # 25–375

REAGENT or RESOURCE	SOURCE	IDENTIFIER
40 μm filter	Genesee Scientific	Cat # 25–376
Tamoxifen	Cayman Chemical	Cat# 13258–1G
IMDM	GIBCO	Cat # 12440053
RPMI	Lonza	Cat# 12–115F
Liberase	Roche	Cat #5401020001
HBSS	Lonza	Cat# 10–527F
HEPES (1M)	Corning	Cat # 25–60CI
Penicillin-Streptomycin	Life Technologies	Cat# 15140–122
2x SensiFAST probe No-ROX mix	Bioline	Cat # BIO-86005
PMA (Phorbol myristate acetate)	Sigma	Cat# P8139–1MG
Ionomycin	Sigma	Cat # I0634–1 MG
Brefeldin A	Sigma	Cat # B6542–5MG
H_2O_2	Sigma	Cat# W4502–1L
REAGENT or RESOURCE	SOURCE	IDENTIFIER
Tween Buffered Saline (TBS)	Alfa Aesar	Cat # 77–86-1
Tween-20	Acros Organics	Cat # 23336–2500
Peroxidase streptavidin	Jackson Immuno Research	Cat #016–030-084
Alexa Fluor 594 Tyramide Reagent	Invitrogen	Cat # B40957
Mouse-on-Mouse blocking reagent	Vector labratories	Cat # BMK-2202
DAPI (4',6-diamidino-2-phenylindole, dihydrochloride)	Sigma	Cat # D9542–10MG
ACK lysis buffer	Life Technologies	Cat # A10492–01
Experimental models: Mouse strains		
mdx (C57BL/10ScSn-Dmdmdx/J)	The Jackson Laboratory	Cat #001801
YetCre13 (C.129S4(B6)-Il13tm1(YFP/cre)Lky/J)	The Jackson Laboratory	Cat # 017353
DTA (B6.129P2-Gt(ROSA)26Sortm1(DTA)Lky/J)	The Jackson Laboratory	Cat # 009669
Red5 (B6(C)-N5tm1.1(icre)Lky/J)	The Jackson Laboratory	Cat # 030926
Rosa26-DUX4(B6.129S6-Gt(ROSA)26Sortm1(DUX4) Sqh/J)	The Jackson Laboratory	Cat # 032779
HSA-mER-CRE-mER (Tg(ACTA1-Cre/Esr1*)2Kesr/J)	The Jackson Laboratory	Cat # 025750
Critical commercial assays		
Quick-RNA Microprep kit	Zymo Research	Cat # R1050
Quick-RNA Miniprep kit	Zymo Research	Cat # R1054
SensiFAST cDNA synthesis kit	Bioline	Cat # BIO-65053
eBioscience Foxp3/Transcription Factor Staining Buffer Set	Thermo Fisher Scientific	Cat # 00–5523-00
Avidin/biotin blocking kit	Vector Laboratories	Cat # SP-2001
Oligonucleotides		
Taqman Assays for qPCR, See Table S2	This paper	N/A
Mouse genotyping primers; See Table S3	This paper	N/A
Software and algorithms		

REAGENT or RESOURCE	SOURCE	IDENTIFIER
Prism (Version 8.4)	GraphPad	https://www.graphpad.com/scientific-software/prism/
FlowJo (Version 10.4)	BD Biosciences	https://www.flowjo.com/
FIJI - ImageJ	Schindelin et al., 2012	https://imagej.net/Fiji
QuantiMus (Version 1.0)	Kastenschmidt et al., 2019	https://quantimus.github.io/